frontiers | Frontiers in Earth Science

ORIGINAL RESEARCH
published: 24 May 2022
doi: 10.3389/feart.2022.921988

Effects of Fracture Formation Stage on Shale Gas Preservation Conditions and Enrichment in Complex Structural Areas in the Southern Sichuan Basin, China

Jing Li[1], *Hu Li*[2,3,4,5]*, *Jianliang Xu*[1], *Yijia Wu*[1,4] *and Zhi Gao*[1]

[1]Institute of Geological Exploration and Development of CNPC Chuanqing Drilling Engineering, Chengdu, China, [2]Natural Gas Geology Key Laboratory of Sichuan Province, Southwest Petroleum University, Chengdu, China, [3]Shale Gas Evaluation and Exploitation Key Laboratory of Sichuan Province, Chengdu, China, [4]School of Geoscience and Technology, Southwest Petroleum University, Chengdu, China, [5]Department of Railway Engineering, Sichuan College of Architectural Technology, Chengdu, China

Fractures have significantly impacted the preservation, enrichment, and productivity of shale gas in the Longmaxi Formation in the complex structural area of the southern Sichuan Basin. Based on outcrop, core, imaging logging, inclusion analysis, acoustic emission experiments, and burial and thermal evolution history data, the formation stage, evolution and preservation conditions of structural fractures were comprehensively studied. Shear fractures are the main features of tectonic origin and are characterized by small widths, wide spacing, and high filling degrees. The structural fractures of the Longmaxi Formation can be divided into three groups in terms of their formation stage. The first-stage fractures were formed in the middle-late period of the Yanshanian tectonic movement (86.2–68.5 Ma), when the palaeotectonic stress was 68.33–71.82 MPa; and the homogenization temperature of the fluid inclusions in the corresponding fracture fillings is 150–178°C. The second-stage fractures were formed at the end of the Yanshanian -early Himalayan tectonic movement (68.5–35.2 Ma), when the palaeotectonic stress was 85.2–100.5 MPa; the homogenization temperature of the corresponding fluid inclusions is 123–148°C. The third-stage tectonic fractures formed during the middle-late period of the Himalayan tectonic movement (35.2–0 Ma), when the palaeotectonic stress was 55.6–63.8 MPa; fillings are scarce in these fractures, but the measured homogenization temperature of the corresponding fluid inclusions is 90–110°C. Shale gas preservation conditions were affected by the fracture formation stage, maximum horizontal crustal stress, fault scale, structural burial depth, formation pressure coefficient, etc. Three types of favourable preservation conditions were identified. The Type I target area is the low slope area in the middle of the syncline, which occurs more than 2.0 km from the fault. The research results have guiding significance for the evaluation of the preservation conditions of deep shale gas in the study area and similar areas.

Keywords: deep shale gas, accumulation geological conditions, formation stage, structural fracture, shale gas preservation conditions, southern Sichuan basin

OPEN ACCESS

Edited by:
Jingshou Liu,
China University of Geosciences Wuhan, China

Reviewed by:
Zhu Baiyu,
Yangtze University, China
Gaoyuan Sun,
Hohai University, China

***Correspondence:**
Hu Li
lihu860628@126.com

Specialty section:
This article was submitted to Structural Geology and Tectonics, a section of the journal Frontiers in Earth Science

Received: *17 April 2022*
Accepted: *09 May 2022*
Published: *24 May 2022*

Citation:
Li J, Li H, Xu J, Wu Y and Gao Z (2022) Effects of Fracture Formation Stage on Shale Gas Preservation Conditions and Enrichment in Complex Structural Areas in the Southern Sichuan Basin, China. Front. Earth Sci. 10:921988. doi: 10.3389/feart.2022.921988

1 INTRODUCTION

The Wufeng Formation-Longmaxi Formation Section One in the Sichuan Basin is rich in shale gas resources, with a geological resource volume of 21.9×10^{12} m^3, of which deep shale gas from the burial depths of 3,500–4,500 m accounts for 51%, i.e., 11.3×10^{12} m^3. The volume shale gas resources in southern Sichuan is 10×10^{12} m^3, of which the 8.7×10^{12} m^3 from burial depths of 3,500–4,500 m accounts for 87% (Ma et al., 2018; Wei et al., 2019; Ma et al., 2021; Li et al., 2022a; 2022b). Breakthroughs have been achieved in exploring and developing shale gas in the middle to shallow layers of the southern Sichuan Basin, and shale gas commercial development zones, such as Changning, Weiyuan, and Zhaotong, have been established (Liu et al., 2016; Li et al., 2019a; Fan et al., 2020a; Hou et al., 2020; Tang et al., 2020; Wang et al., 2020; Li et al., 2022a). Shale gas exploration and development is progressing in the deep (burial depths greater than 3,500 m) shale gas areas of Luzhou and Yuxi in the southern Sichuan Basin. The test gas production of Well Y 101 (Yang, vertical depth 3,577 m) is 43×10^4 m^3/d, representing a breakthrough of deep shale gas. The test daily gas production of Well Z202-H1 (Zu, vertical depth 3,960 m) is 46×10^4 m^3, and the test gas production of Well L203 (Lu) has reached 138×10^4 m^3/d, which indicates the great potential of deep shale gas exploration and development at depths of 3,500–4,500 m in the southern Sichuan Basin (Guo J. et al., 2021; Wang et al., 2021; Xi and Tang 2021).

Many scholars have proposed that marine shale in southern China has experienced multiple stages of tectonic activity and a lengthy evolutionary history and is characterized by an old deposition age, a complex genesis, strong tectonic activity, and variable gas-bearing properties (Fan et al., 2020b; Liu H. et al., 2022a; Zhang et al., 2022). The development of faults and fractures under effective preservation conditions is key for determining the quality of shale gas reservoirs (Xie 2021; Li et al., 2022a; Li et al.,2022b; Liu J. S. et al., 2022b). Due to the extremely low permeability of shale formations, fractures not only serve as storage spaces but also improve porosity and permeability and connect pores and microstructures, thereby playing a vital role in controlling underground gas migration (Li et al.,2022b). Qualitative and quantitative research has been conducted on naturally formed shale fractures and the fracture networks formed after fracturing stimulation, the relationship between fractures and permeability, the propagation of fractures during hydraulic fracturing, and the mechanisms of fracture formation, which are crucial features to understand to improve gas enrichment and accumulation, reservoir performance, and production capacity (Liu et al., 2018, 2020, 2021; Li H. et al., 2021a, Li H. T. et al., 2021; Qie et al., 2021; Wang et al., 2021; Wang and Wang 2021; Zhan et al., 2021). The characteristics, formation stages and genetic mechanisms of natural fractures in shale reservoirs play an important role in controlling and regulating the migration and accumulation of shale gas (Fan et al., 2018; Gao 2019; Nie et al., 2020; Kang 2021; He et al., 2022a; 2022b). Taking the Longmaxi Formation of the Luzhou area in the southern Sichuan Basin as an example, this study analyses the main tectonic evolution stages, structural fracture formation stages, and fracture formation mechanisms by using macroscopic geological methods (interpretations of outcrop, drilling, and geophysical data) and microexperimental tests (analysis of fluid inclusions from fracture fillings, acoustic emission experimental results, and the burial and thermal evolution history). The research results provide guidance for the high-quality exploration and development of deep shale gas in complex structural areas in southern Sichuan and can help improve well placement optimization, fracturing stimulation optimization, and productivity predictions.

2 REGIONAL GEOLOGIC BACKGROUND

The Luzhou block is located in a low and steeply dipping structural belt in southern Sichuan, surrounded by the gently dipping structural belt of central Sichuan, the high and steeply dipping structural belt of eastern Sichuan, the low-folded structural belt of southwestern Sichuan and the Loushan fold belt. The Luzhou block primarily contains NE-trending structures and broom-like structures from NE to SW, where the strength of the structural folds gradually weakens (Jin et al., 2018; Ma et al., 2018). The Luzhou block is primarily characterized by wide synclines and narrow anticlines, and contains three large-scale synclines. The Luzhou block has two groups of main faults that trend NE-SW and E-W, and the distance between the main faults is large, which controls the tectonic shape (**Figure 1A**). There are 32 Grade I faults in total, and Grade II and III faults are also developed in this region. The fault spacings are generally 20–170 m, and the lengths are generally 5–10 km. The Longmaxi Formation shale in the Luzhou block has multistage, multitype, and multidirectional natural fracture systems, which are important for enriching and accumulating shale gas, improving reservoir performance, and predicting productivity.

During the sedimentary period of the Longmaxi Formation, the entire southern Sichuan area was bounded by the central Sichuan palaeo-uplift and the central Guizhou palaeo-uplift, and generally was a continental shelf sedimentary environment. The Luzhou block was located in the sedimentary depocentre of the deep-water continental shelf sedimentary centre during the sedimentary period of the Wufeng Formation-Longmaxi Formation. The bottom of the Longmaxi Formation conformably contacts the Wufeng Formation, and the top of the Longmaxi Formation contacts the carbonate rocks of the lower Silurian Shiniulan Formation (Xie et al., 2019; Guo J. L. et al., 2020a; Guo X. S. et al., 2020b). The high-quality shale section at the bottom of the Longmaxi Formation is rich in biogenic siliceous minerals with a mass fraction of 60–70%, characterized by the shale total organic carbon (TOC) mass fraction of 2.8–6.0% (an average of 3.9%), a porosity of 4.0–6.5% (an average of 5.1%), and a gas saturation of 50–70% (an average of 65%) (**Figure 1B**). The total gas content tested in the field is 5.0–7.5 m^3/t with an average of 6.3 m^3/t, which is the highest in southern Sichuan.

3 FAVOURABLE TARGET PRESERVATION CONDITIONS FOR DEEP SHALE GAS

3.1 Samples

This study primarily focuses on two methods, i.e., macrogeological analysis and microexperimental testing.

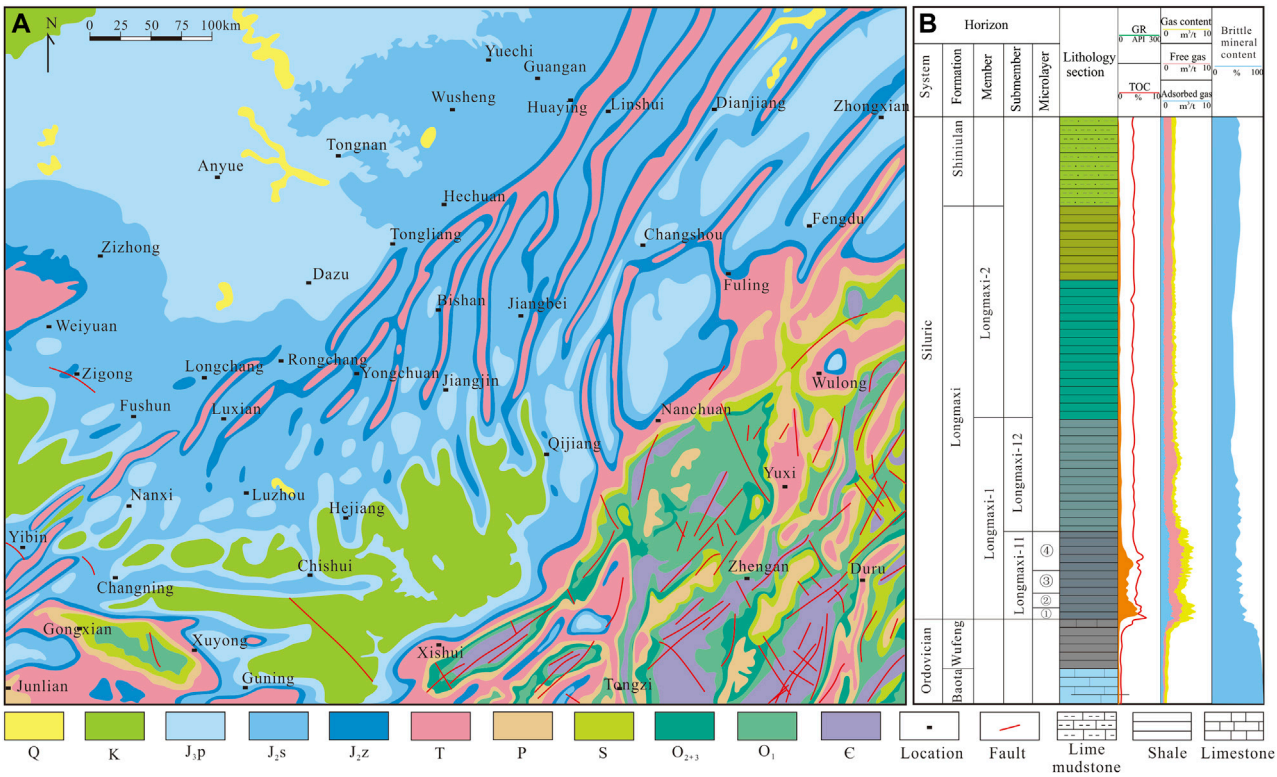

FIGURE 1 | Geological setting of the Luzhou block. **(A)**. Structural location; **(B)**. Comprehensive stratigraphic diagram.

Macroscopic geological analysis primarily uses surface structure analysis, drilling core observations, Formation Micro Imager (FMI) logging interpretations and seismic structure analysis, which were conducted in combination with the analysis of actual production data. Observations and sampling were conducted on the cores at approximately 320 m from four wells drilled in the Longmaxi Formation, including Well L201, Well L203H79-4, Well Y101H3-8, and Well Y101H41-2. A total of 48 samples of fracture fillings and 15 full-diameter samples were observed. FMI logs of the 12 wells encountering the Longmaxi Formation, including Well L206, Well L211, and Well Y101H3-8, were collected and interpreted, and 3D seismic data from the Luzhou shale gas production area (covering 1,470 km^2) were collected, analysed, and interpreted.

3.2 Macrogeological Analysis

The surface structural analysis primarily used the regional structural background to determine the fracture stage and to classify surface faults in the Luzhou area. The drilling core observations mainly included the fracture type, development degree, filling characteristics, and fracture intersection relationship, and the fracture occurrence was primarily determined and interpreted with FMI logging. The LANDMAK 2003.12.13 interpretation system and 10 × 10 density controls were used to process and interpret the 3D seismic data and to study the fault distribution, intersection relationships, and evolution processes at different stages.

3.3 Microexperimental Tests

The fracture stages were studied by macroscopic fracture analysis and the analysis of structural fractures formed at the same stage as the fractures. Rock mechanics tests on the Longmaxi Formation cores, homogenization temperature tests of the fluid inclusions in the fracture fillings, and the burial history of the study area were used to determine the fracture formation stage (Fan et al., 2020a).

Rock slices from 30 fracture fillings of five wells in the study area were placed on a Linkam THMSG600 stage at room temperature, and the microscope was focused to find the inclusions. During heating, when the inclusions were close to homogenization, the heating rate was changed to 1–3°C/min. When the gas-liquid phase in the inclusions transformed into a homogeneous phase, the homogenization temperature was obtained, and the fluid filling stage was obtained according to the homogenization temperature test of the fluid inclusions.

The rock mechanics tests were completed by the Rock Mechanics Laboratory of the State Key Laboratory of Oil and Gas Reservoir Geology and Exploitation, Southwest Petroleum University. The tests included triaxial compression tests and acoustic emission tests. The acoustic emission test primarily uses the memory characteristics of unfractured rocks. When the pressure conditions approach those of the tectonic stress that occurred during geologic history, the unfractured rocks break, resulting in acoustic emission effects, which can be used to determine the tectonic stress stage. In this study, samples were collected in three directions, i.e., 0°, 45°, and 90°, from 15 full-

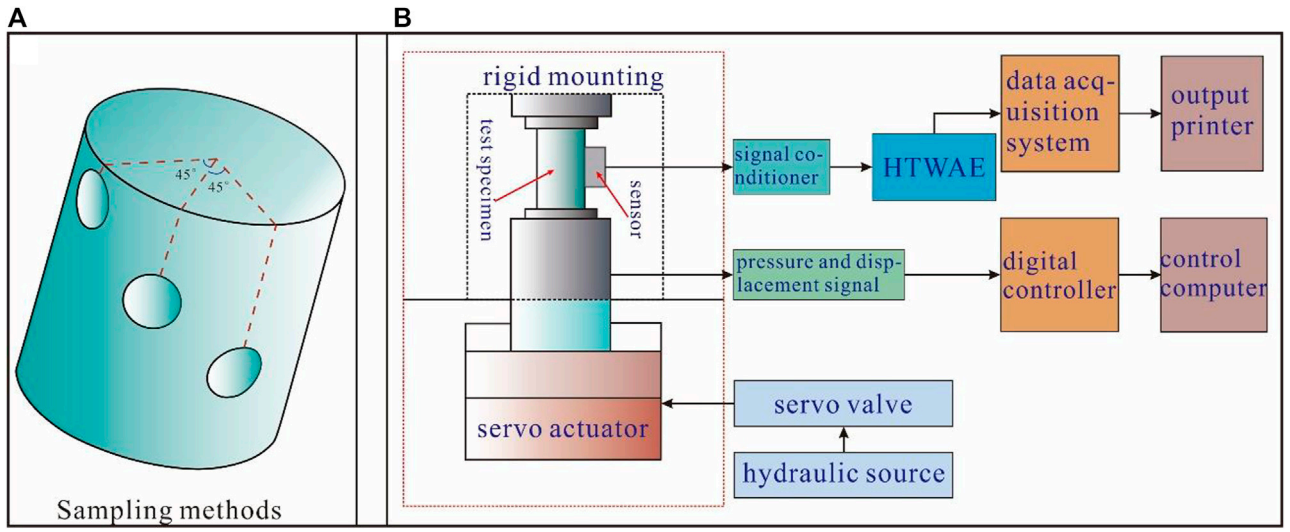

FIGURE 2 | Rock acoustic emission testing experimental system. **(A)**. Sampling methods; **(B)**. Experiment process.

diameter cores to create cylindrical samples 50 mm × 25 mm in size (**Figure 2A**). The rock mechanical parameters of the samples were measured using the RTR-1000 high-temperature and high-pressure triaxial rock mechanics test system produced by GCTS (**Figure 2B**) (Fan et al., 2022). The tests were performed in accordance with GB/T 23561.11-2009, GB/T 50266-2013, SY/T5336-2006, and SY/T 6351-1998.

The duration and intensity of tectonic deformation were studied based on the experimental results obtained from the burial thermal evolution history of core samples from the Luzhou area, and the experimental data were provided by the Sichuan Shale Gas Exploration and Development Company.

4 FAVOURABLE TARGET PRESERVATION CONDITIONS FOR DEEP SHALE GAS

4.1 Fracture Stage Study With Macrogeological Methods

4.1.1 Analysis of Surface Structures

The southern margin of the Sichuan Basin is influenced by the Jiangnan Xuefeng uplift belt, the Daliangshan fault-fold structural belt, and the Daloushan fault-fold structural belt. The right triangular joint structural area in southern Sichuan is bounded and connected by the Changshou-Zunyi fault zone, the Gulin-Yanjin fault zone, and the Huayingshan-Qingshanling fault zone. Constrained by the surrounding structures, the boundary structure trajectory is consistent with the boundary extension orientation, and strong superposition and transformation occur inside the basin. The study area is located at the intersection of the southern Sichuan fold belt and Loushan fault-fold structural belt and has been transformed by structural activities that have occurred at different stages and in different directions; therefore, the area exhibits structural compounding and superposition characteristics in some stages (**Figure 3**).

The folds in this area are divided into three belts, i.e., E-W-trending structural belts, S-N-trending structural belts, and NE-trending structural belts. The E-W-trending structural belt primarily includes the Shengdengshan and Luoguanshan anticlines. This structural belt exhibits an E-W-trending disjointed distribution, and the W end of the main axis often shifts to the S in the WSW direction and is dominated by steeply dipping and low gently dipping tectonic types. The N-S-trending structural belt is primarily located in the Yanggaosi anticline, exhibits a N-S-trending westward protruding arc distribution, with high to low steeply dipping anticlines in the N and low and gently dipping anticlines in the S, and is characterized by a steep slope in the W and a gentle incline in the east. The NE-trending structural belt mainly includes the Gufoshan, Jiukuishan, Huangguashan, Longdongping, and Tanziba anticlines. The main trend of this tectonic belt is to the NE, and the structure is distributed in echelon, arc, and "S" shapes. The NE-trending structural belt is dominated by high overturned, high steeply dipping, and low steeply dipping, which extend to the SE. Judging from the fault development, most of the faults trend NE and near-E-W, and a few NW-trending faults are developed in and around the study area. The extension direction of each fault is approximately the same as that of the fold in which it is located. The main structure in the Luzhou area is directed approximately E-W and turns eastward to the NNW; it has obvious structural superposition characteristics. The NNW structure is superimposed onto the early EW structure, and the tectonic trajectories of adjacent areas are quite different. The NE-trending structure can be observed from the NW direction and was formed due to the influence from the Huayingshan fault zone.

4.1.2 Core Fracture Stage and Classification

The core fracture morphology, filling and intersection relationships provide an intuitive basis for the study of

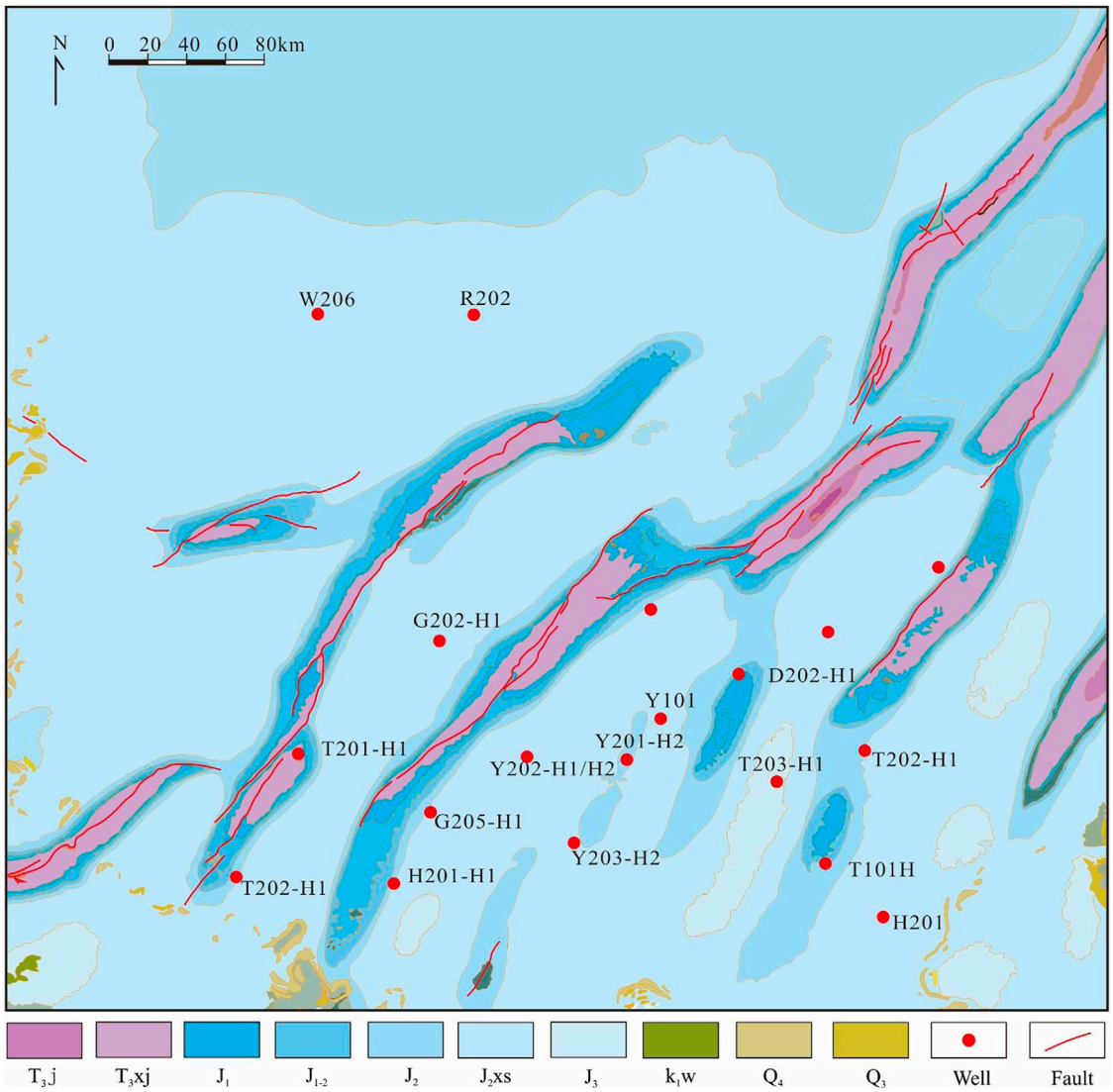

FIGURE 3 | Surface geological map of the Luzhou block.

fracture stages. In the Wufeng Formation-Longmaxi Formation, shear fractures are the primary features of tectonic origin, followed by extensional fractures, shear-tensional fractures and interlayer fractures, as well as a small number of artificially induced fractures. The shear fractures are mostly composed of high-angle shear fractures and vertical fractures, have large extension lengths and straight joint surfaces, and are mostly filled with calcite (**Figures 4A,B**) (Li et al., 2019b; Li H. et al., 2021a; Li H. T. et al., 2021). According to the mutual intersection relationships among core fractures, there are at least three stages of fractures in the Longmaxi Formation (**Figures 4C–F**).

The fractures in the Longmaxi Formation with lengths of 15–25 cm account for 34.5% of the total fractures. The fractures with lengths of 5–15 cm account for the next-largest proportion. Fractures longer than 25 cm are less common. Fractures with widths between 0.5 and 1 mm account for 50% of the total fractures; fractures with widths <0.5 mm account for approximately 14% of the total fractures. Thus, these fractures have small widths. Additionally, they are relatively closed. The Wufeng Formation-Longmaxi Formation fracture density ranges from 3/0.5 m to 10/0.5 m. High-angle fractures (45°–75°) and near-vertical fractures (75°–90°) are dominant. The proportion of unfilled fractures is approximately 26.2%, the proportion of partially fractures is approximately 22.7%, and the proportion of fully filled fractures is approximately 51.1%. Fracture fillings include calcite, pyrite, quartz, and organic matter, etc., indicating a good sealing effect in this area.

The fracture strike orientation interpreted by FMI logging shows that the Well L206 area primarily contains reticulated fractures, mainly NW-trending (330° ± 10°) fractures, followed by NE-trending (30° ± 5°) and NEE-trending (70° ± 5°) fractures. The Well Y101 area primarily contains reticulated fractures, mainly in the NNE (20° ± 10°), NE (40° ± 10°), and ENE (80° ± 10°) directions,

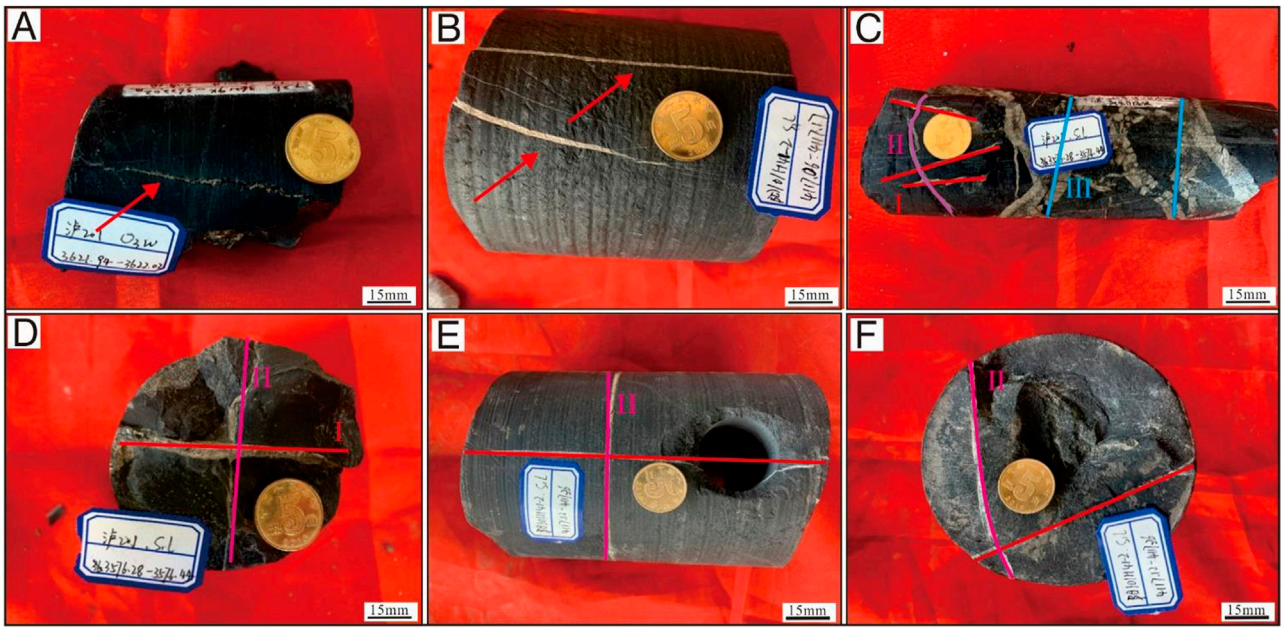

FIGURE 4 | Intersection relationship of typical core fractures of Longmaxi formation in Luzhou block.

followed by near S-N (0° ± 10°) fractures. The Well L211 area primarily contains unidirectional fractures, mainly ENE (80° ± 10°) fractures (**Figure 5**). High-angle fractures and vertical fractures are dominant, and the fracture dip angle mainly ranges from 30° to 80°, which is consistent with the core observation results. According to the fracture dip angle distribution histogram, the fractures observed in the wells in the study area are generally high-angle fractures, followed by near-vertical fractures, with fewer low-angle fractures, and virtually no horizontal fractures.

Based on the occurrence, filling characteristics and mutual intersection relationships among core fractures, at least three stages of structural fractures can be determined, indicating that fracture formation was influenced by at least three stages of tectonic movement.

4.1.3 Stage Classification of Underground Faults

Geophysical interpretations show that the faults in the study area were mostly formed in a large-scale compressional orogenic environment during the Himalayan period and are mainly reverse faults (**Figure 6**). Vertically, the transition zone is composed of the Jialingjiang Formation gypsum rock, thick Silurian Longmaxi mudstone, and Cambrian Gaotai Formation gypsum rock; therefore, three sets of fault systems were formed. The faults extension shape of the main fault system in the Luzhou block trends NE-SW and NE; ENE and NNE trends are also present, which shows that the fault systems in this area did not develop at the same time. Instead, they are the result of multiple stages of tectonic events that occurred in different directions. The bottom boundary of the Late Ordovician Wufeng Formation in the Luzhou area has experienced three stages of tectonic compression in different directions over its geological history. Combined with the morphological features of its surface structures and seismic data from this area, it is believed that the faults, such as those exposed at Wells T40, L28, L34, L40, G11, G35, YS10, and H2, trend ENE in general, whereas those in the NW part of the area trend WE. These faults were the earliest formed and are Stage I faults that formed due to the compressive crustal stress that trends SSE. The overall strike of the L20, Q6, L18, Y35, and other faults is in the NE direction; these faults formed next and Stage II faults that occurred due to the NW compressive crustal stress. Faults, such as those encountered at Wells T15, T30, YS12, DS3, YS11, and YS12, trend N-S overall and were the last faults formed; they are Stage III faults that occurred due to the compressive crustal stress that trends E-W.

4.2 Characteristics of Fluid Inclusions in Fracture Fillings

4.2.1 Types and Homogenization Temperature Characteristics of Fluid Inclusions

The tectonic activities that occurred in different periods may have produced multistage faults. As fluid migration channels, faults can capture fluids with different properties. Inclusions retain information, such as the temperature and pressure when the fluid was captured, thereby retaining traces of tectonic activities at different stages (Nagarajan et al., 2007; He et al., 2018; Fan et al., 2020a). The fracture fluid inclusions in the Silurian Longmaxi Formation primarily include four types of single-phase liquid hydrocarbon inclusions, gas-liquid two-phase hydrocarbon inclusions, single-phase brine inclusions, and two-phase brine inclusions. Inclusions composed of liquid hydrocarbons, ranging in size from 3 μM to 6 μM, are yellow and yellow-green under fluorescence. The size of gas-liquid two-phase inclusions ranges from 4 μM to 10 μM, and the liquid phase is yellow under fluorescence, while the gas phase is colourless under fluorescence. The brine inclusions include single-

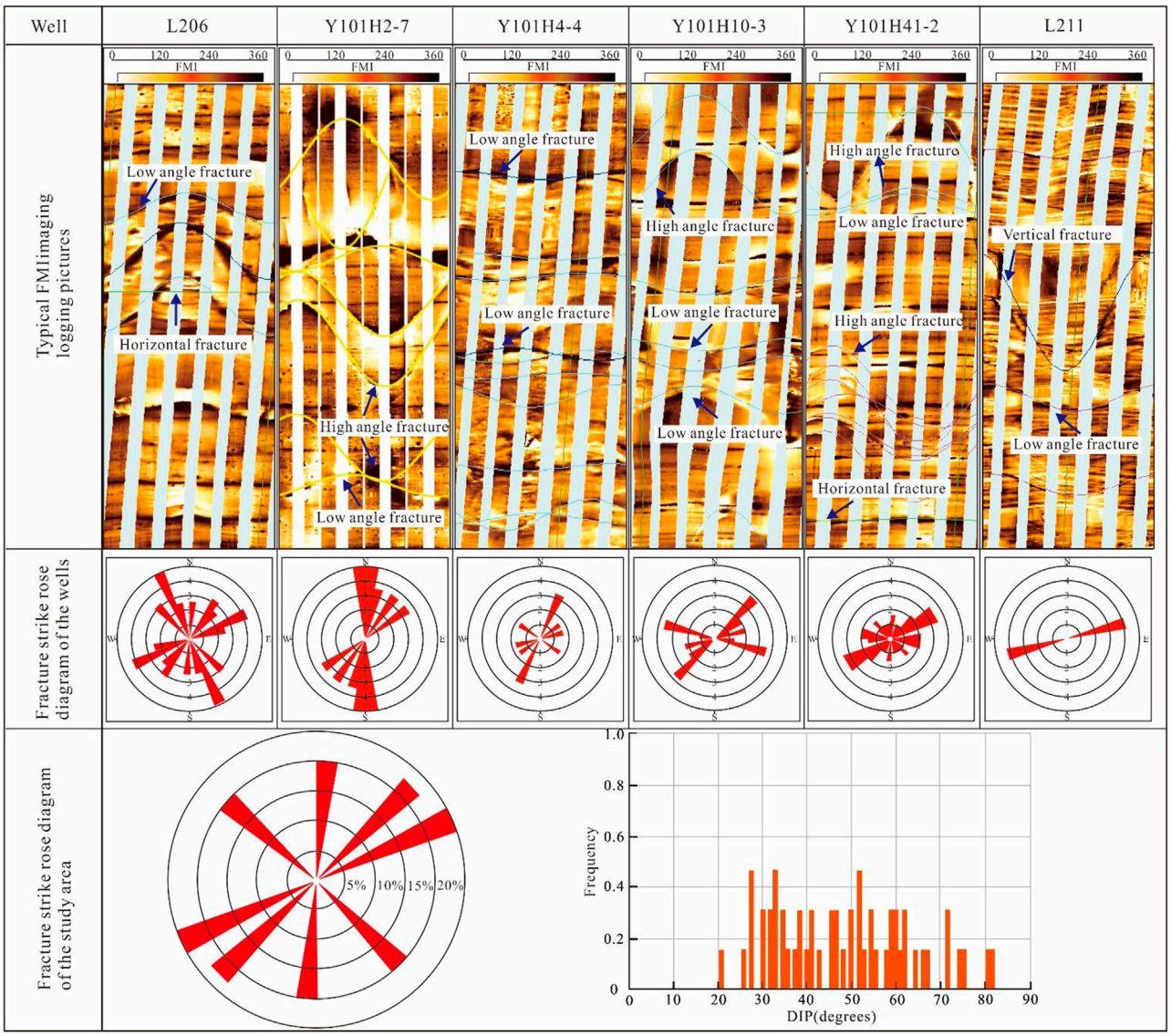

FIGURE 5 | Identification of fracture occurrence based on imaging logging.

phase brine inclusions and two-phase brine inclusions, and the size of the inclusions range from 2 μM to 10 μM (**Table 1**; **Figure 7**).

The test results of the fluid inclusion samples from fracture fillings in L201, L203H79-4, Y101H41-2, and Y101H3-8 show that fluid charging activities in the fractures experienced at least three stages (**Figure 8**). The study area experienced at least three stages of relatively strong tectonic compression before fault and fracture systems were formed, which provided migration channels and charging sites for fluids. The first stage corresponds to the first-stage structural uplift that occurred after the Luzhou area reached its maximum burial depth, and the temperature of inclusions formed at this time is the highest. The inclusions formed during this event include both gas and brine inclusions, and the homogenization temperature of these inclusions is 150–178°C. The second stage corresponds to the temporary uplift of the structure that occurred at the end of the Middle Triassic due to the Indosinian event; the inclusions formed during this event are brine inclusions from the same period of the asphalt formation, and the fluid charging homogenization temperature caused by the short-term uplift is mainly 123–148°C. The third stage corresponds to the period from the mid-Himalayan orogeny to the present day, which is the structural setting period, during which slow uplift lasted for an extended period. The inclusions formed during this stage are oil and bitumen inclusions, and the homogenization temperature of these fluid inclusions is 90–110°C.

4.2.3 Indicative Significance of Inclusions for Preservation Conditions

The inclusions in Well L201 are dominated by high-density liquid hydrocarbon inclusions and high density methane inclusions,

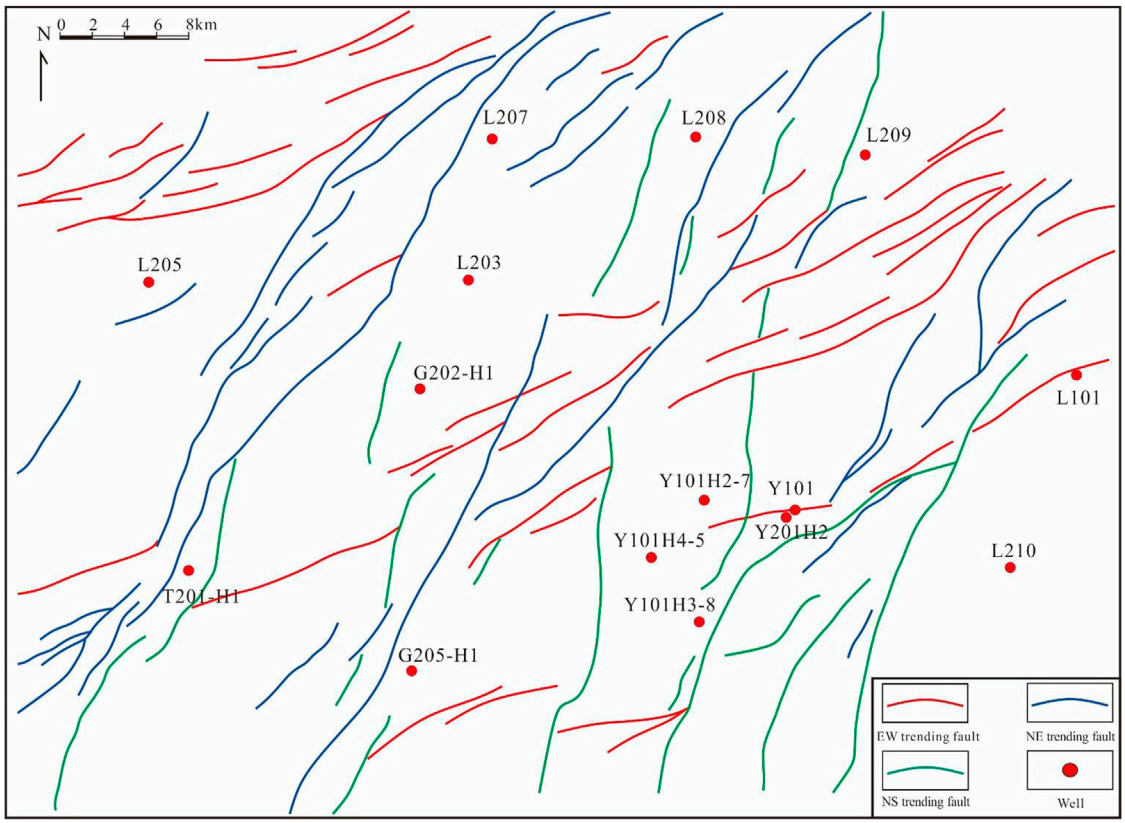

FIGURE 6 | Distribution of the fault system in the Longmaxi Formation of the Luzhou block.

indicating that the fractures in Well L201 were formed at the time of the maximum burial depth of the shale. Hydrocarbon inclusions in the high-quality shale sections are highly developed, while two-phase inclusions are very rare, and low-temperature two-phase inclusions are less rare, indicating that the fluid activity in the late stage of structural fractures was weak (Burruss et al., 1983; Mourgues et al., 2012; Han et al., 2018). The brine inclusions are dominant in Well L203H79-4 and Y101H3-8, which also include a small number of hydrocarbon inclusions and carbonaceous bitumen inclusions, indicating that 1) fluid inclusions were not developed during the stage of massive oil and gas generation, and the homogenization temperature of the hydrocarbon inclusions is between 123 and 155°C; 2) during the uplift and denudation stage, fluid inclusions were developed and influenced by filling by external water, and the homogenization temperature of brine inclusions is between 98 and 112°C. In the geologic history of Well Y101H41-2, brine inclusions are dominant and coexist with gas inclusions. These inclusions have homogenization temperatures between 90 and 114°C and are characterized by low-temperature fluids, which represent the filling of formation fluids. Oil and gas deposits were captured during the generation period, and the inclusions developed during this period were primarily brine inclusions, indicating a high degree of shale gas loss across geological history. The multistage homogenization temperatures of the shale fluid inclusions reveal subsequent multiple structural fractures and fluid charging events. The vertical distribution of fluid inclusion types includes brine inclusions at the bottom and a small amount of hydrocarbon inclusions at the top, indicating that the deep fluids intruded upwards into the high-quality shale intervals along fractures, and that shale gas escaped from the bottom layers.

The fluid inclusion types present in L201, L203H79-4, Y101H3-8, and Y101H41-2 indicate that the preservation conditions of shale gas in this area gradually deteriorated from W to E, which is consistent with the strength of the regional tectonic deformation.

4.3 Fracture Formation Stages Determined by Acoustic Emission Experiments

The Kaiser effect of the acoustic emission test was evaluated for five groups of 15 samples in the study area, and the number of effect points that appeared on the acoustic emission experimental curve was used to determine the stages of tectonic compression experienced during the geohistorical period. The acoustic emission energy accumulation-time relationship and stress-time relationship curves were established (Suboyin et al., 2020; Qiu et al., 2021; Shan et al., 2021; Song et al., 2021; Xi et al., 2021). The energy accumulation-time relationship curve shows that as the load gradually increased, the energy suddenly increased at 50 s; after that, there were four sharp energy accumulation points,

TABLE 1 | Test data of fluid inclusions in fracture fillings of the Longmaxi Formation (partial).

Well	No.	Depth	Distribution characteristics	Distribution form	Size/μM	Gas- liquid ratio/%	Homogenization temperature/°C
L201	1	3576.28	Zonal distribution	Irregular	7	8	108
	2	3576.28			10	10	120
	3	3576.28			6	8	114
	4	3576.28			6	5	135
	5	3576.28		Strip	7	4	150
	6	3766.00		Oval	5	4	142
	7	3766.00			5	4	164
	8	3766.00			8	8	178
L203H79-4	9	3797.95		Irregular	12	6	98
	10	3816.72		Triangle	8	6	123
	11	3825.26		Irregular	7	6	115
	12	3826.88			8	6	148
	13	3846.20		Diamond	9	6	155
	14	3846.88		Strip	9	5	108.3
	15	3872.66			8	5	114.3
	16	3900.62		Irregular	7	5	128.7
Y101H3-8	17	3279.83		Oval	6	6	112
	18	3279.83		Irregular	5	5	108
	19	3754.44			6	6	135
	20	3742.48		Strip	8	6	126
	21	3772.84		Irregular	6	5	118
	22	3772.84			6	5	100
Y101H41-2	23	3779.36		Rectangle	5	6	90
	24	3782.95		Oval	5	4	114
	25	4117.12			4	5	105
	26	4126.00		Irregular	4	4	101
	27	4126.00			5	4	112
	28	4143.62			7	4	109.6

and a total of five high-energy accumulation points (**Figure 9**). Four obvious inflection points, namely, the characteristic points of the Kaiser effect, can be seen on the energy accumulation-time relationship curve. The experimental results show that five Kaiser effect points can be identified on the energy accumulation-time curve of multiple samples from the Longmaxi Formation in the Luzhou area, reflecting that the rock has experienced five microfracture events throughout geologic history. According to the stress pattern of the rock acoustic emission measurements, the palaeotectonic stresses corresponding to the five Kaiser effect points are as follows: Caledonian tectonic stress of 26.5–32.03 MPa, mid-late Yanshanian tectonic stress of 68.3–76.8 MPa, late Yanshanian-early Himalayan tectonic stress of 85.2–100.5 MPa, middle-late Himalayan tectonic stress of 55.6–63.8 MPa, and present stress field value of 46.8–56.2 MPa.

Combining with the existing research results and regional tectonic evolution history in and around the study area, the five stages of tectonic stress in this study area are as follows: the present tectonic stress, the mid-Himalayan-present tectonic stress, the late Yanshanian-early Himalayan tectonic stress, the mid-late Yanshanian tectonic stress, and the Caledonian tectonic stress stages, respectively. Because the Caledonian tectonic event included up-and-down movement throughout the entire southern Sichuan region, it had little effect on the fracture development and structural trajectory, and the tectonic motion at this stage can be excluded from the explanation of fracture development. The comprehensive analysis of the regional tectonic evolution history shows that the study area has experienced at least three stages of tectonic motion since the Late Ordovician and at least three corresponding fracture development stages. The three periods in which these three-stage fractures developed are the middle-late Yanshanian period, the end Yanshanian period-early Himalayan period, and the middle Himalayan period-present.

5 DISCUSSION

5.1 Structure and Hydrocarbon Evolution of Shale Gas Reservoirs

In general, the Luzhou area is characterized by three stages, i.e., formation of shale gas reservoirs in the early stage, enrichment of high-pressure and ultrahigh-pressure shale gas in the middle stage, and small uplift and denudation in the later stage. The duration and magnitude of structural uplift can be obtained by analysing the burial thermal history. The maximum burial depth in the Luzhou area was 6,020–6,635 m, the uplift range was 2087–2,353 m, and the uplift occurred at 78–85 Ma. The shale has experienced three stages of burial (hydrocarbon generation) and three stages of uplift. Burial stage I of the Wufeng Formation-Longmaxi Formation shale in typical wells in the Luzhou area was the rapid burial that occurred from the Late Ordovician to late early Silurian. This stage corresponds to the early to middle stage of oil generation; the burial depth was more than 2 km, and the formation temperature was approximately

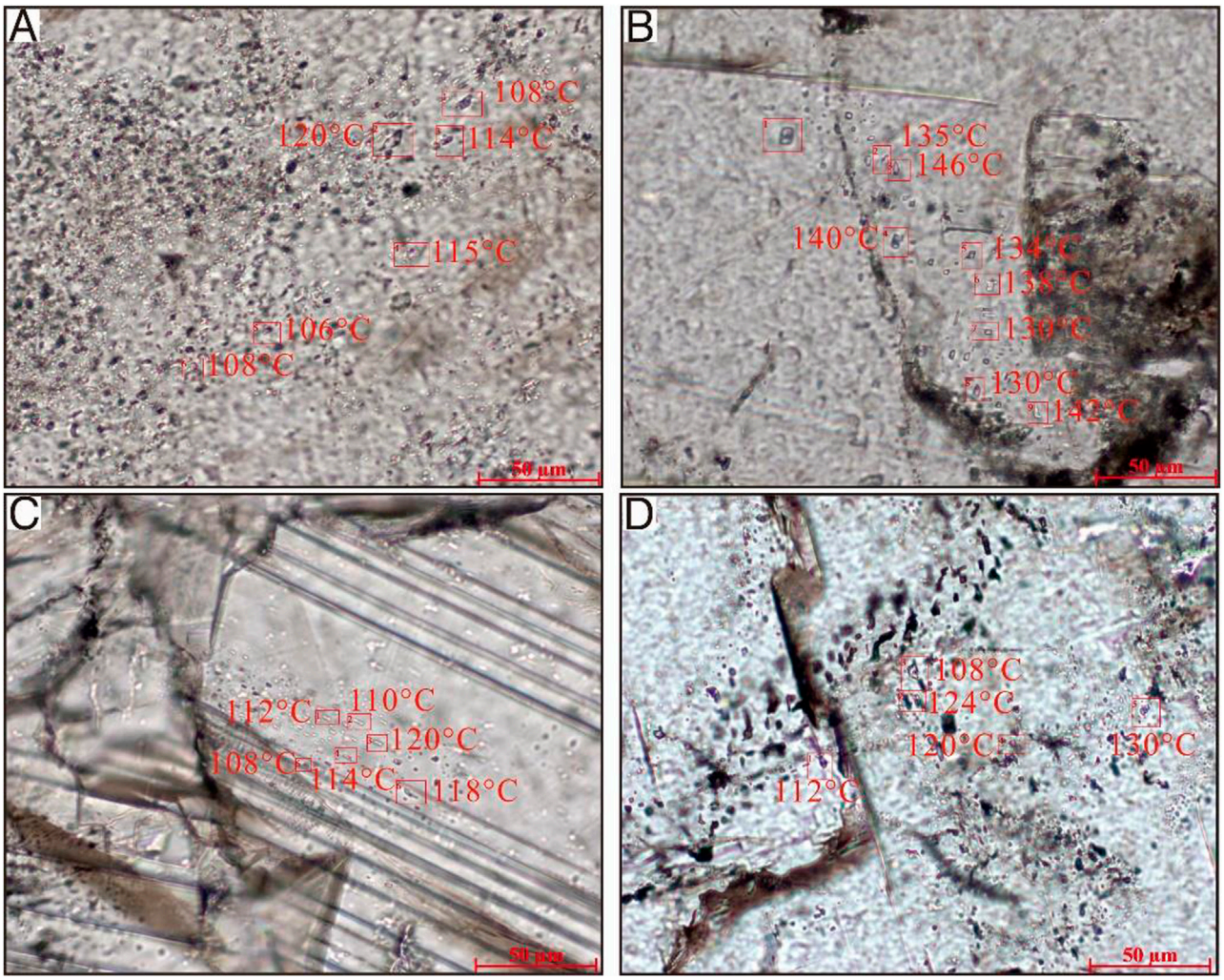

FIGURE 7 | Fluid inclusions in typical fracture fillings of the Luzhou block. **(A)**, **(B)**. Well L201, 3,576.28, Longmaxi Formation; **(C)**. Well L206, 4043.20, Longmaxi Formation; **(D)**. Well Y101H3-8, 3779.36, Longmaxi Formation.

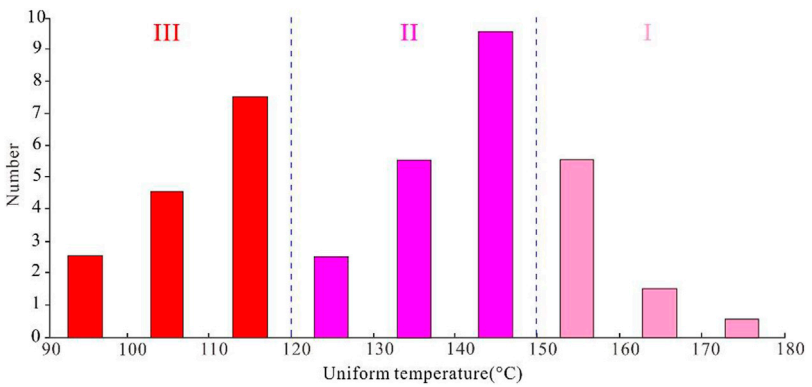

FIGURE 8 | Homogeneous temperature distribution of fluid inclusions in fracture fillings of the Luzhou block.

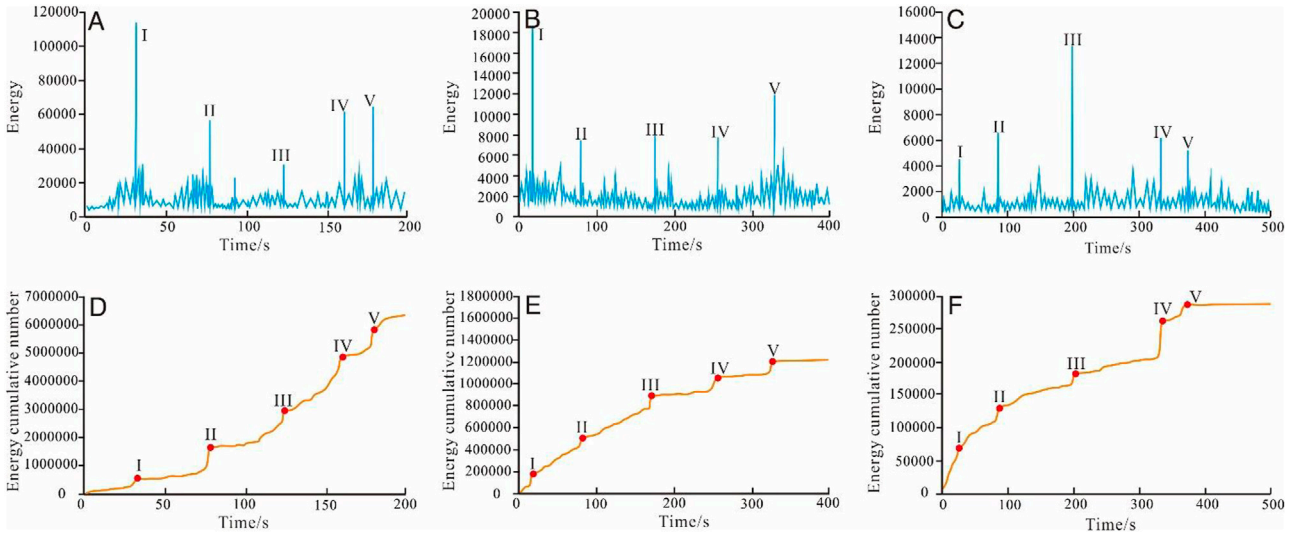

FIGURE 9 | Acoustic emission experimental results of the Well L203H79-4 (3842.81–3843.16 m). **(A)**, **(D)**. The sampling angle is 0°; **(B)**, **(E)**. The sampling angle is 45°; **(C)**, **(F)**. The sampling angle is 90°.

90–110°C. Uplift stage I (oscillatory uplift) included the slow uplift from the end of the middle Silurian to the Carboniferous. Burial stage II included the sedimentary deposition and subsidence that occurred during the early Permian-Early Triassic and corresponds to a burial depth of nearly 3 km and a formation temperature of approximately 130–170°C. This stage is the later stage of oil generation, during which organic matter began to generate and expel hydrocarbons in large quantities, and the vitrinite reflectance (Ro) of samples from this period was between 0.7% and 1.0%. Uplift stage II (short-term uplift) was the short-term uplift of the structure at the end of the Middle Triassic that occurred due to the influence of the Indosinian event. Burial stage III featured a rapid and deep burial from the Middle Triassic to the late Cretaceous, to a burial depth of approximately 6,273 m, and the formation temperature exceeded 200°C. The organic matter entered the high-overmature stage, and the Ro values from samples from this period are approximately 1.3%–3.0% (**Figure 10**). Various types of organic matter preserved in shale began to decompose during this period; therefore, this stage is the primary gas generation stage. Uplift stage III (transformation and uplift period) was influenced by the uplift of the Qinghai-Tibet Plateau in the Himalayas and the depression of the western Sichuan foreland basin that has occurred since the Late Cretaceous. Rapid uplift and transformation occurred from the Late Cretaceous to the Neogene, and uplift occurred at approximately 75–85 Ma. The shale is deeply buried and has developed multistage fault deformation, and the enrichment and preservation conditions of the shale gas are still optimal, with relatively large total resources and a relatively high abundance.

The degree of thermal evolution of organic matter is usually quantitatively characterized by the Ro value, and a moderate degree of thermal evolution can promote shale gas enrichment. The test results of the equivalent Ro value of organic matter in shale samples from the Luzhou area show that the thermal evolution of organic matter generally exceeds 2.0%, and the equivalent Ro value ranges from 2.86% to 3.34% (an average of 3.16%). The organic matter in the Luzhou area is at the stage of high-overmature pyrolysis and can produce dry gas, which ensures that the organic matter has been converted into hydrocarbons. During the thermal evolution of shale, when the degree of thermal evolution and Ro values are less than the "critical point", at Ro values between 2.8 and 3.2%, the is between 0.6 and 6.3%, and the porosity is between 2.8 and 5.8%. The porosity and pore structure characteristics of shale reservoirs are controlled by other factors, such as organic carbon content, clay mineral types, and thermal evolution degree, among which the thermal evolution degree is a key factor. As the shale Ro increases, the rate of hydrocarbon generation in the shale increases, a large amount of natural gas is generated, and elliptical or stomata-shaped overpressure-induced organic pores are formed. When the thermal evolution degree (Ro) is greater than 3.2%, the porosity is between 2.7% and 5.7% (**Figure 11A**), and the TOC is between 0.4% and 5.5%; additionally, the porosity of shale slowly decreases as the Ro value increases (**Figure 11B**). The continued thermal evolution of the shale reservoirs leads to organic matter graphitization, during which the pore structure of the shale changes, organic pores collapse, the specific surface areas of several meso- to micropores in the reservoirs decrease, and the specific surface areas of organic pores in the shale decrease.

5.2 Fracture Development Stages and Evolution Models

The main fault system in the Luzhou area trends NE-SW, NE, ENE and NNE, which indicates that the fault system in this area is the result of multistage tectonic compression that occurred in different directions. By comprehensively analysing the results

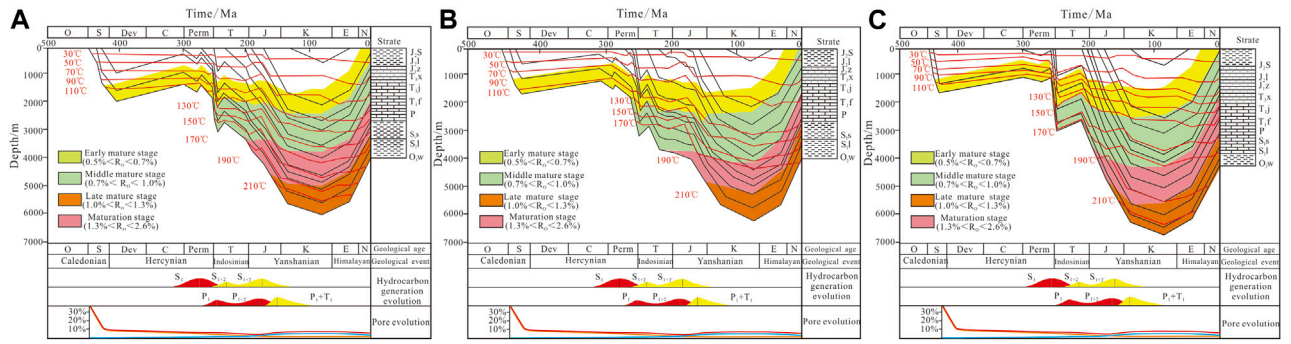

FIGURE 10 | Comprehensive model of burial history, hydrocarbon generation and structural evolution of shale in the Longmaxi formation encountered in typical wells in the Luzhou area. **(A)**. Well Y101H65-5; **(B)**. Well L205; **(C)**. Well 201.

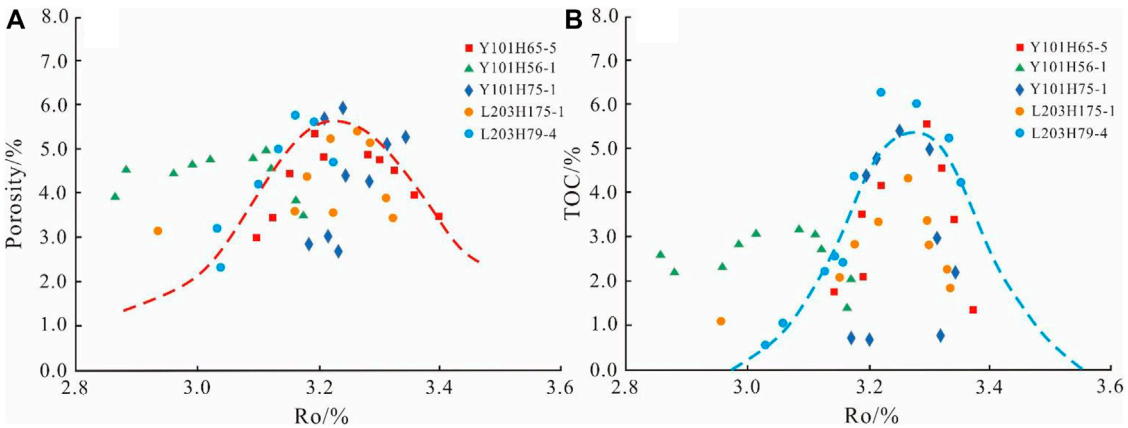

FIGURE 11 | Evolution of shale organic matter in the Longmaxi Formation of the Luzhou area. **(A)**. Relationship between R_O and porosity; **(B)**. Relationship between R_O and TOC.

from the rock acoustic emission experiments, inclusion homogenization temperature testing and burial-thermal evolution history (Li et al., 2019b), it was confirmed that the Longmaxi Formation in the Luzhou area experienced three major tectonic events; therefore, the formation of surface and underground fractures is also divided into three stages (**Figure 12**).

During the middle-late period of the Yanshan Movement (86.2–68.5 Ma), the Luzhou area was squeezed from the S to the N by the Daloushan tectonic belt, and the maximum effective principal stress was 76.8 MPa, resulting in WNW-trending conjugate plane shear fractures and NE- and near-E-W-trending conjugate shear fractures, among which the near-EW-trending conjugate shear fractures further expanded and penetrated into new areas, forming near-EW-trending faults with the earliest formation stage, i.e., the Stage I faults. The palaeotectonic stress of the tectonic motion at this stage was 68.3–76.8 MPa. The resulting fractures were formed early and have a high degree of filling. The filling material is mostly calcite, and the homogenization temperature of the fluid inclusions in these fillings is 150–178°C.

From the end of the Yanshan Movement to the middle of the Himalayan Movement (68.5–35.2 Ma), the uplift of the Qinghai-Tibet Plateau triggered the NW-SE extrusion in this area. The maximum effective principal stress was 100.5 MPa, forming NW-trending and nearly E-W-trending conjugate plane shear fractures and NE-trending conjugate shear fractures, of which the NE-trending conjugate shear fractures further expanded and penetrated, forming many NE-trending faults with the second-earliest formation stage, i.e., the Stage II fractures. The palaeotectonic stress at this stage was 86.91–99.61 MPa, and the resulting fractures have a high degree of filling. The fillings are mostly calcite, with a small amount of pyrite, and the homogenization temperature of the fluid inclusions in these fillings is 123–148°C.

From the late Himalayan Movement to the present (35.2–0 Ma), due to the combined action of the Jiangnan Xuefeng uplift and the central Sichuan uplift, the Luzhou area was squeezed by the resultant force in the E-W direction, and the maximum effective principal stress was 63.8 MPa, forming NNE-trending conjugate plane shear fractures and near-N-S-trending conjugate shear fractures, of which the near-NS-trending

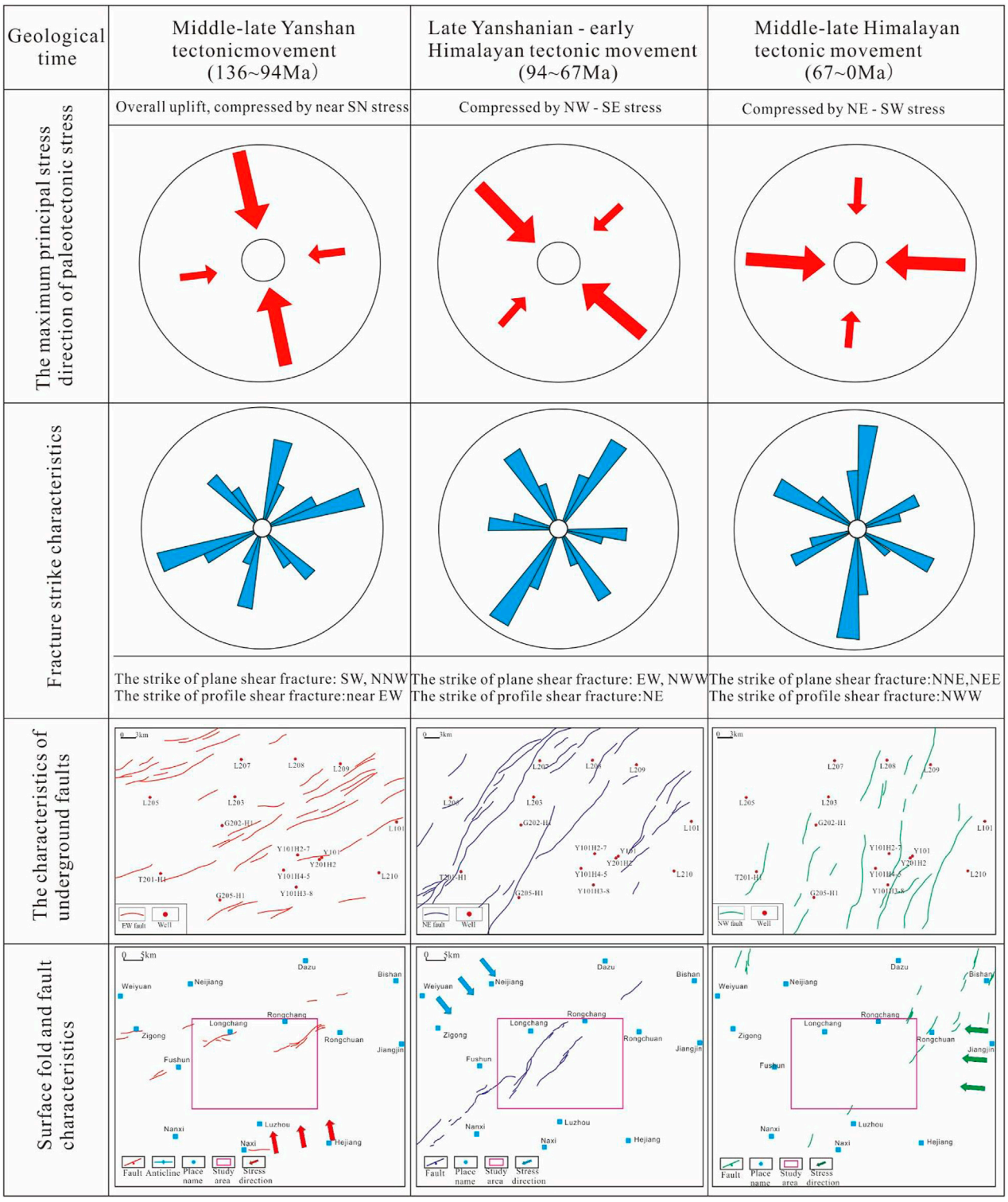

FIGURE 12 | Fracture and fault evolution model for the Longmaxi Formation of the Luzhou area.

conjugate shear fractures further extended and penetrated, forming a large number of near-N-S-trending fractures during the latest formation stage, i.e., the Stage III faults. The palaeotectonic stress of tectonic movement at this stage was 47.76–57.64 MPa, and the resulting fractures have a low filling degree. The filling materials are mostly a small amount of calcite

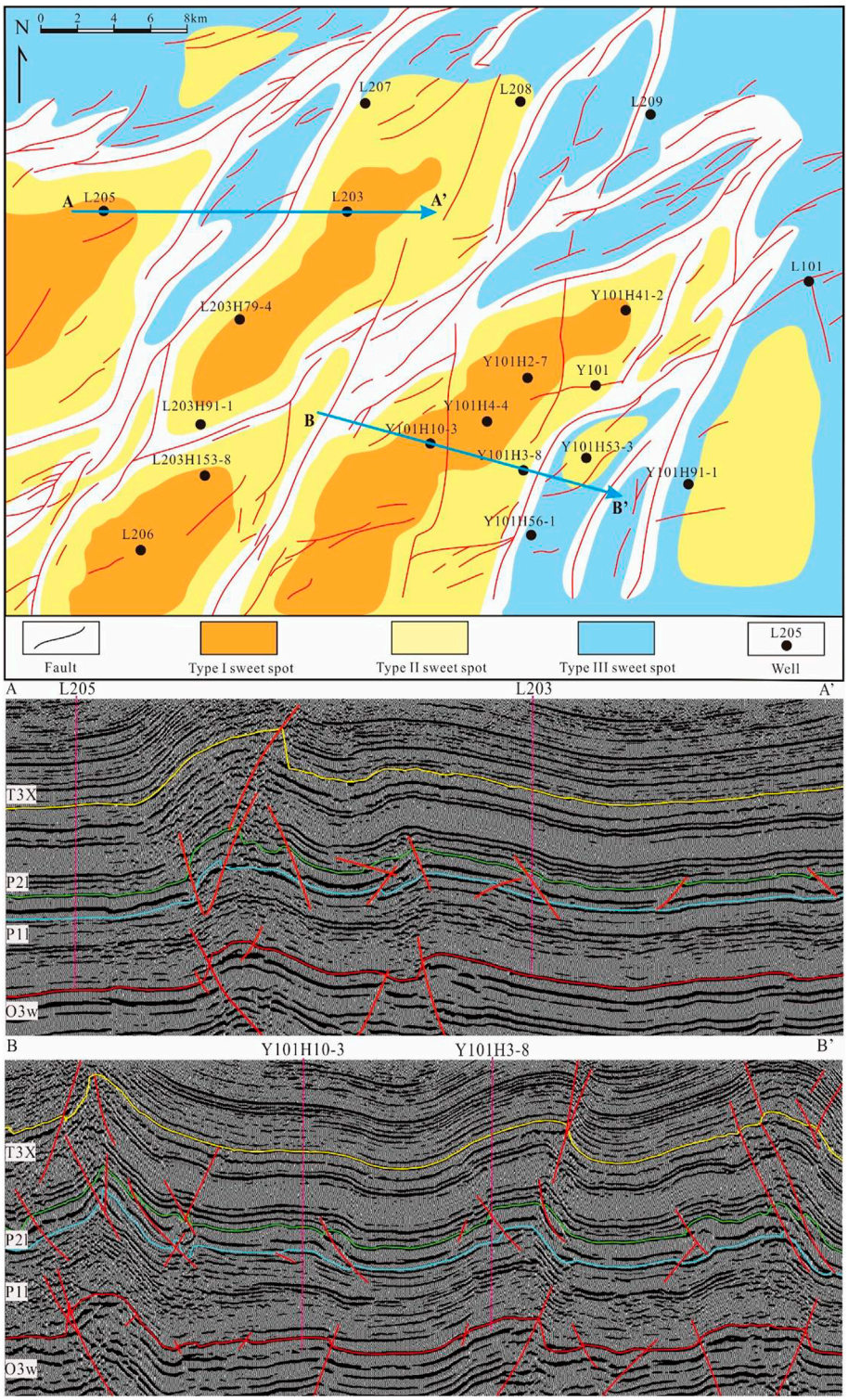

FIGURE 13 | Favourable area for shale gas preservation in the Luzhou area.

and mud, and the homogenization temperature of the fluid inclusions in these fillings is 90–110°C.

5.3 Effect of the Fracture Stage on Shale Gas Preservation and Enrichment

The tectonic movement caused fractures to form in the Longmaxi Formation. The dominant orientations and development degrees of fractures formed at different tectonic evolution stages are different, and the effects on the enrichment of the shale gas and the gas-bearing properties of the shale in the later stage are also different (Curtis 2002; Yin et al., 2019; Guo W. X. et al., 2021). The direction of the maximum horizontal principal stress in the Longmaxi Formation is ESE at each well in the Luzhou block. Within the range of 105° ± 10°, the fault stage is related to the maximum horizontal crustal stress, which is one of the important influencing factors of oil and gas preservation conditions. In general, the mid-late Yanshan tectonic movement intensity is small, mainly involving vertical up-and-down movement, and the fault scale is small. The formation of the Stage I ENE- and E-W-trending fractures occurred early, and the resulting fractures have a high degree of filling, but the angle between the fracture direction and the current crustal stress orientation is small, which has a certain influence on shale gas dissipation. The scales and distributions of Stage II NE-trending faults that formed at the end of the Yanshan Movement to the middle of the Himalayan Movement are quite different from those of the Stage I fractures. Both sides of the NE-trending faults were subjected to the ESE-trending stress, causing lateral displacement along the fault strike and forming a certain extensional environment. As a result, the sealing performance of the faults is reduced, resulting in a reduction in the ability to preserve oil and gas. Stage III N-S-trending faults that formed from the late Himalayan Movement to the middle stage of the present are squeezed and closed under the action from the ESE-trending stress, forming an overall compressive environment. The N-S-trending, NNE-trending and NE-trending fractures exhibit a large angle (>20° or more) to the current crustal stress direction (105 ± 10°) and are more likely to improve the gas-bearing properties of the shale. The development of small-scale and medium-scale fractures has little effect on the oil and gas preservation capacity in the study area.

Oil and gas preservation conditions are affected by factors such as fault stage and maximum horizontal crustal stress, fault scale, structural burial depth, and formation pressure coefficient. A quantitative target evaluation system and standard for shale gas sweet spots were established, and three types of favourable preservation conditions were identified (**Figure 13**). The Type I sweet spot area is affected by the faults and is concentrated in the southwest of the Well Lu 205, Well Lu 203, and Well Yang 101 areas; it belongs to the middle area of a broad and gentle syncline in structure, and the spacing of the Stage II NE-trending faults is more than 2.0 km; here, the shale gas preservation conditions are good, the formation pressure coefficient is between 2.0 and 2.2, the shale burial depth is between 3,500 and 4,000 m, and the stress difference coefficient is as low as 0.12–0.16. The favourable areas for oil and gas preservation in the Type II sweet spot area are mostly distributed in a ring-shaped zone in the slope area in the transition from syncline to anticline; the spacing of the Stage II NE-trending faults is 1.0–2.0 km, the preservation conditions of shale gas are weakened to a certain extent, the pressure coefficient is 2.0–2.1, the shale burial depth is 3,500–4,000 m, and the stress difference coefficient is 0.16–0.18. The Type III sweet spot areas are mostly concentrated in the middle and northern areas of the block and the structurally high structural parts of the anticline; here, the formation pressure coefficient is between 1.9 and 2.1, the shale burial depth is 3,000–3,500 m, and the stress difference coefficient is high (0.16–0.20); faults and folds have developed in the corresponding areas, and the spacing of the Stage II NE-trending fault is less than 1.0 km. The oil and gas preservation conditions of the Longmaxi Formation in the northern Well Lu 207, Well Lu 208, and Well Lu 209 areas are generally poor.

6 CONCLUSION

(1) Due to its tectonic history, the Longmaxi Formation is primarily composed of high-angle fractures and vertical fractures. The fractures have a small width, large spacing, and high filling degree, and their conductivity is poor. The Longmaxi Formation was primarily influenced by tectonic compression in the three directions of SSE, NW, and W-E after sedimentation, and the fractures mostly developed in the NW direction (330° ± 10°), NE direction (30° ± 5°), and ENE direction (70° ± 5°).

(2) The formation of structural fractures of the Longmaxi Formation in the Luzhou area can be divided into three stages. The first-stage fractures were formed in the middle-late period of the Yanshanian tectonic movement (86.2–68.5 Ma) with a palaeotectonic stress of 68.33–71.82 MPa, and the corresponding homogenization temperature of the fluid inclusions in fracture fillings is 150–178°C. The second-stage fractures were formed at the end of the Yanshanian-early Himalayan tectonic movement (68.5–35.2 Ma) with a palaeotectonic stress of 85.2–100.5 MPa, and the corresponding homogenization temperature is 123–148°C. The formation time of the third-stage fractures is the middle-late period of the Himalayan tectonic movement (35.2–0 Ma) with a palaeotectonic stress of 55.6–63.8 MPa. The filling degree of these fractures is low, and the corresponding homogenization temperature is 90–110°C.

(3) Fractures with an early formation time, high filling degree, and a larger angle between the fracture orientation and the current crustal stress orientation are favourable for preserving shale gas. Otherwise, shale gas preservation conditions may be easily damaged. Shale gas preservation conditions are affected by the fault stage, maximum horizontal crustal stress, fault scale, structural burial depth, and formation pressure coefficient. Three types of favourable preservation conditions were identified. The Type I area belongs to the middle area of a broad and gentle syncline, which is concentrated in the southwestern part of the Well L205, Well L203, and Well Y101 areas.

DATA AVAILABILITY STATEMENT

The original contributions presented in the study are included in the article/supplementary material, further inquiries can be directed to the corresponding author.

AUTHOR CONTRIBUTIONS

JL and HL contributed in writing, reviewing, and editing, datacuration, writing—original draft preparation; JX, YW, and ZG contributed in formal analysis, validation, and reviewing.

FUNDING

This study was financially supported by the Open Funds of Natural Gas Geology Key Laboratory of Sichuan Province (No. 2021trqdz05) and Shale Gas Evaluation and Exploitation Key Laboratory of Sichuan Province (No. YSK2022002).

ACKNOWLEDGMENTS

We thank all editors and reviewers for their helpful comments and suggestions.

REFERENCES

Burruss, R. C., Cercone, K. R., and Harris, P. M. (1983). Fluid Inclusion Petrography and Tectonic-Burial History of the Al Ali No. 2 Well: Evidence for the Timing of Diagenesis and Oil Migration, Northern Oman Foredeep. *Geology* 11, 567–570. doi:10.1130/0091-7613(1983)11<567:fipath>2.0.co;2

Curtis, J. B. (2002). Fractured Shale-Gas Systems. *AAPG Bull.* 86 (11), 1921–1938. doi:10.1306/61eeddbe-173e-11d7-8645000102c1865d

Fan, C. H., He, S., Zhang, Y., Qin, Q. R., and Zhong, C. (2018). Development Phases and Mechanisms of Tectonic Fractures in the Longmaxi Formation Shale of the Dingshan Area in Southeast Sichuan Basin, China. *Acta Geol. Sin.* 92 (6), 2351–2366.

Fan, C., Li, H., Zhao, S., Qin, Q., Fan, Y., Wu, J., et al. (2020a). Formation Stages and Evolution Patterns of Structural Fractures in Marine Shale: Case Study of the Lower Silurian Longmaxi Formation in the Changning Area of the Southern Sichuan Basin, China. *Energy fuels.* 34, 9524–9539. doi:10.1021/acs.energyfuels.0c01748

Fan, C., Li, H., Qin, Q., He, S., and Zhong, C. (2020b). Geological Conditions and Exploration Potential of Shale Gas Reservoir in Wufeng and Longmaxi Formation of Southeastern Sichuan Basin, China. *J. Pet. Sci. Eng.* 191, 107138. doi:10.1016/j.petrol.2020.107138

Fan, C. H., Xie, H. B., Li, H., Zhao, S. X., Shi, X. C., Liu, J. F., et al. (2022). Complicated Fault Characterization and its Influence on Shale Gas Preservation in the Southern Margin of the Sichuan Basin, China. *Lithosphere* 2022, 8035106. doi:10.2113/2022/8035106

Gao, F. Q. (2019). Use of Numerical Modeling for Analyzing Rock Mechanic Problems in Underground Coal Mine Practices. *J. Min. Strata Control Eng.* 1 (1), 013004. doi:10.13532/j.jmsce.cn10-1638/td.2019.02.009

Guo, J. L., Jia, C. Y., He, D. B., Li, L., Zhu, H. Q., Zhou, Y., et al. (2020a). Classified Evaluation of Shale Reservoirs in the Ordovician Wufeng to Silurian Longmaxi Formations in the Southern Sichuan Basin. *Geol. J. China Univ.* 26 (3), 323–332. doi:10.16108/j.issn1006-7493.2019047

Guo, X. S., Hu, D. F., Huang, R. C., Wei, Z. H., Duan, J. B., Wei, X. F., et al. (2020b). Deep and Ultra-deep Natural Gas Exploration in the Sichuan Basin: Progress and Prospect. *Nat. Gas. Ind.* 40 (5), 1–14. doi:10.1016/j.ngib.2020.05.001

Guo, J., Jia, C., He, D., and Meng, F. (2021a). Classification and Evaluation on Shale Gas Reservoir for Wufeng-Longmaxi Formation in Chuannan Area, Sichuan Basin. *Lithosphere* 2021, 3364731. doi:10.2113/2021/3364731

Guo, W. X., Tang, J. M., Ouyang, J. S., Wang, T., Wang, X., and Wang, Y. (2021b). Characteristics of Structural Deformation in the Southern Sichuan Basin and its Relationship with the Storage Condition of Shale Gas. *Nat. Gas. Ind.* 41 (5), 11–19. doi:10.3787/j.issn.1000-0976.2021.05.002

Han, Z.-Z., Liu, H., Song, Z.-G., Zhong, W.-J., Han, C., Han, M., et al. (2018). Geochronology, Geochemistry, and Tectonic Implications of Upper Silurian - Lower Devonian Meta-Sedimentary Rocks from the Jiangyu Group in Eastern Jilin Province, Northeast China. *Can. J. Earth Sci.* 55, 490–504. doi:10.1139/cjes-2017-0260

He, Z. L., Li, S. J., Nie, H. K., Yuan, Y. S., and Wang, H. (2018). The Shale Gas "Sweet Window": "The Cracked and Unbroken" State of Shale and its Depth Range. *Mar. Pet. Geo.* 101, 334–342. doi:10.1016/j.marpetgeo.2018.11.033

He, S., Qin, Q. R., Li, H., and Zhao, S. X. (2022a). Geological Characteristics of Deep Shale Gas in the Silurian Longmaxi Formation in the Southern Sichuan Basin, China. *Front. Earth Sci.* 9, 818543. doi:10.3389/feart.2021.818155

He, S., Qin, Q. R., Li, H., and Wang, S. L. (2022b). Deformation Differences in Complex Structural Areas in the Southern Sichuan Basin and its Influence on Shale Gas Preservation: A Case Study of Changning and Luzhou Area. *Front. Earth Sci.* 9, 818155. doi:10.3389/feart.2021.818534

Hou, E. K., Cong, T., Xie, X. S., and Wei, J. B. (2020). Ground Surface Fracture Development Characteristics of Shallow Double Coal Seam Staggered Mining Based on Particle Flow. *J. Min. Strata Control Eng.* 2 (1), 013521. doi:10.13532/j.jmsce.cn10-1638/td.2020.01.002

Jin, Z., Nie, H., Liu, Q., Zhao, J., and Jiang, T. (2018). Source and Seal Coupling Mechanism for Shale Gas Enrichment in Upper Ordovician Wufeng Formation - Lower Silurian Longmaxi Formation in Sichuan Basin and its Periphery. *Mar. Petroleum Geol.* 97, 78–93. doi:10.1016/j.marpetgeo.2018.06.009

Kang, H. P. (2021). Temporal Scale Analysis on Coal Mining and Strata Control Technologies. *J. Min. Strata Control Eng.* 3 (1), 013538. doi:10.13532/j.jmsce.cn10-1638/td.20200814.001

Li, H., Tang, H. M., and Zheng, M. J. (2019a). Micropore Structural Heterogeneity of Siliceous Shale Reservoir of the Longmaxi Formation in the Southern Sichuan Basin, China. *Minerals* 9, 548. doi:10.3390/min9090548

Li, H., Tang, H., Qin, Q., Zhou, J., Qin, Z., Fan, C., et al. (2019b). Characteristics, Formation Periods and Genetic Mechanisms of Tectonic Fractures in the Tight Gas Sandstones Reservoir: A Case Study of Xujiahe Formation in YB Area, Sichuan Basin, China. *J. Pet. Sci. Eng.* 178, 723–735. doi:10.1016/j.petrol.2019.04.007

Li, H., Wang, Q., Qin, Q., and Ge, X. (2021a). Characteristics of Natural Fractures in an Ultradeep Marine Carbonate Gas Reservoir and Their Impact on the Reservoir: A Case Study of the Maokou Formation of the JLS Structure in the Sichuan Basin, China. *Energy fuels.* 35, 13098–13108. doi:10.1021/acs.energyfuels.1c01581

Li, H. T., Peng, R., Du, W. S., Li, X. P., and Zhang, N. B. (2021b). Experimental Study on Structural Sensitivity and Intervention Mechanism of Mechanical Behavior of Coal Samples. *J. Min. Strata Control Eng.* 3 (4), 043012. doi:10.1638/td.20210820.001

Li, J., Qin, Q., Li, H., and Zhao, S. (2022a). Paleotectonic Stress Field Modeling and Fracture Prediction of the Longmaxi Formation in the N216 Well Block, Southern Sichuan Basin, China. *Arab. J. Geosci.* 15, 347. doi:10.1007/s12517-022-09616-z

Li, J., Qin, Q., Li, H., Wan, Y., and Wan, Y. F. (2022b). Numerical Simulation of the Stress Field and Fault Sealing of Complex Fault Combinations in Changning Area, Southern Sichuan Basin, China. *Energy Sci. Eng.* 10 (2), 278–291. doi:10.1002/ese3.1044

Li, H. (2022a). A Review of Mechanical Mechanism and Prediction of Natural Fracture in Shale. *Arab. J. Geosci.* 15 (6), 474. doi:10.1007/s12517-022-09786-w

Li, H. (2022b). Research Progress on Evaluation Methods and Factors Influencing Shale Brittleness: A Review. *Energy Rep.* 8, 4344–4358. doi:10.1016/j.egyr.2022.03.120

Liu, S. G., Deng, B., Zhong, Y., Ran, B., Yong, Z. Q., Sun, W., et al. (2016). Unique Geologic Features of Burial and Superimposition of the Lower Paleozoic Shale□gas across the Sichuan Basin and its Periphery. *Earth Sci. Front.* 23 (1), 11–28. doi:10.13745/j.esf.2016.01.002

Liu, J., Ding, W., Gu, Y., Xiao, Z., Dai, J., Dai, P., et al. (2018). Methodology for Predicting Reservoir Breakdown Pressure and Fracture Opening Pressure in Low-Permeability Reservoirs Based on an *In Situ* Stress Simulation. *Eng. Geol.* 246, 222–232. doi:10.1016/j.enggeo.2018.09.010

Liu, J. S., Yang, H. M., Wu, X. F., and Liu, Y. (2020). The *In Situ* Stress Field and Microscale Controlling Factors in the Ordos Basin, Central China. *Int. J. Rock Mech. Min.* 135, 104488. doi:10.1016/j.ijrmms.2020.104482

Liu, J., Yang, H., Bai, J., Wu, K., Zhang, G., Liu, Y., et al. (2021). Numerical Simulation to Determine the Fracture Aperture in a Typical Basin of China. *Fuel* 283, 118952. doi:10.1016/j.fuel.2020.118952

Liu, H., Ban, S., Bédard, K., and Giroux, B. (2022a). Characteristics of Precambrian Basement Intruded by Cretaceous Geological Intrusions in Monteregian Igneous Province and Their Impacts on Regional Thermal Structure. *Adv. Geo-Energy Res.* 6 (3), 206–220. doi:10.46690/ager.2022.03.04

Liu, J. S., Yang, H. M., Xu, K., Wang, Z. M., Liu, X. Y., Cui, L. J., et al. (2022b). Genetic Mechanism of Transfer Zones in Rift Basins: Insights from Geomechanical Models. *GSA Bull.* doi:10.1130/b36151.1

Ma, Y. S., Cai, X. Y., and Zhao, P. R. (2018). Chinas Shale Gas Exploration and Development: Understanding and Practice. *Pet. Explor. Dev.* 45 (4), 561–574. doi:10.1016/s1876-3804(18)30065-x

Ma, X., Wang, H., Zhou, S., Shi, Z., and Zhang, L. (2021). Deep Shale Gas in China: Geological Characteristics and Development Strategies. *Energy Rep.* 7, 1903–1914. doi:10.1016/j.egyr.2021.03.043

Mourgues, R., Bureau, D., Bodet, L., Gay, A., and Gressier, J. B. (2012). Formation of Conical Fractures in Sedimentary Basins: Experiments Involving Pore Fluids and Implications for Sandstone Intrusion Mechanisms. *Earth Planet. Sci. Lett.* 313-314, 67–78. doi:10.1016/j.epsl.2011.10.029

Nagarajan, R., Madhavaraju, J., Nagendra, R., Armstrong-Altrin, J. S., and Moutte, J. (2007). Geochemistry of Neoproterozoic Shales of the Rabanpalli Formation, Bhima Basin, Northern Karnataka, Southern India: Implications for Provenance and Paleoredox Conditions. *Rev. Mex. Cienc. Geol.* 24, 150–160.

Nie, H. K., He, Z. L., Liu, G. X., Zhang, G. R., Lu, Z. Y., Li, D. H., et al. (2020). Status and Direction of Shale Gas Exploration and Development in China. *China Univ. Min. Technol.* 49 (1), 13–35. doi:10.13247/j.cnki.jcumt.001096

Qie, L., Shi, Y. N., and Liu, J. G. (2021). Experimental Study on Grouting Diffusion of Gangue Solid Filling Bulk Materials. *J. Min. Strata Control Eng.* 3 (2), 023011. doi:10.13532/j.jmsce.cn10-1638/td.20201111.001

Qiu, Z., Song, D., Zhang, L., Zhang, Q., Zhao, Q., Wang, Y., et al. (2021). The Geochemical and Pore Characteristics of a Typical Marine-Continental Transitional Gas Shale: A Case Study of the Permian Shanxi Formation on the Eastern Margin of the Ordos Basin. *Energy Rep.* 7, 3726–3736. doi:10.1016/j.egyr.2021.06.056

Shan, S. C., Wu, Y. Z., Fu, Y. K., and Zhou, P. H. (2021). Shear Mechanical Properties of Anchored Rock Mass under Impact Load. *J. Min. Strata Control Eng.* 3 (4), 043034. doi:10.13532/j.jmsce.cn10-1638/td.20211014.001

Song, J. F., Lu, C. P., Li, Z. W., Ou, Y. G. C., Cao, X. M., and Zhou, F. L. (2021). Characteristics of Stress Distribution and Microseismic Activity in Rock Parting Occurrence Area. *J. Min. Strata Control Eng.* 3 (4), 043518. doi:10.13532/j.jmsce.cn10-1638/td.20210607.002

Suboyin, A., Rahman, M. M., and Haroun, M. (2020). Hydraulic Fracturing Design Considerations, Water Management Challenges and Insights for Middle Eastern Shale Gas Reservoirs. *Energy Rep.* 6, 745–760. doi:10.1016/j.egyr.2020.03.017

Tang, Y., Li, R., and Wang, S. (2020). Research Progress and Prospects of Coal Petrology and Coal Quality in China. *Int. J. Coal Sci. Technol.* 7 (2), 273–287. doi:10.1007/s40789-020-00322-3

Wang, J., and Wang, X. L. (2021). Seepage Characteristic and Fracture Development of Protected Seam Caused by Mining Protecting Strata. *J. Min. Strata Control Eng.* 3 (3), 033511. doi:10.13532/j.jmsce.cn10-1638/td.20201215.001

Wang, X., Tang, Y., Wang, S., and Schobert, H. H. (2020). Clean Coal Geology in China: Research Advance and its Future. *Int. J. Coal Sci. Technol.* 7 (2), 299–310. doi:10.1007/s40789-020-00321-4

Wang, B., Lu, C. L., Huang, Z. K., and Hu, S. Y. (2021). Experimental Study on Damage Evolution Characteristics of Rock under Triaxial Rheological Disturbance. *J. Min. Strata Control Eng.* 3 (4), 043028. doi:10.13532/j.jmsce.cn10-1638/td.20210525.001

Wang, B., Zhou, F., Zhou, H., Ge, H., and Li, L. (2021). Characteristics of the Fracture Geometry and the Injection Pressure Response during Near-Wellbore Diverting Fracturing. *Energy Rep.* 7, 491–501. doi:10.1016/j.egyr.2020.12.039

Wei, D., Liu, H., and Shi, K. (2019). What Are the Key Barriers for the Further Development of Shale Gas in China? A Grey-DEMATEL Approach. *Energy Rep.* 5, 298–304. doi:10.1016/j.egyr.2019.02.010

Xi, Z., and Tang, S. (2021). Geochemical Characteristics and Organic Matter Accumulation of Late Ordovician Shale in the Upper Yangtze Platform, South China. *Energy Rep.* 7, 667–682. doi:10.1016/j.egyr.2021.01.029

Xi, Y., Jiang, J., Li, J., Li, H., and Gao, D. (2021). Research on the Influence of Strike-Slip Fault Slippage on Production Casing and Control Methods and Engineering Application during Multistage Fracturing in Deep Shale Gas Wells. *Energy Rep.* 7, 2989–2998. doi:10.1016/j.egyr.2021.05.039

Xie, J., Qin, Q., and Fan, C. (2019). Quantitative Prediction of Fracture Distribution of the Longmaxi Formation in the Dingshan Area, China Using FEM Numerical Simulation. *Acta Geol. Sin. - Engl. Ed.* 93 (6), 1662–1672. doi:10.1111/1755-6724.13815

Xie, J. T., Fu, X. P., Qin, Q. R., and Li, H. (2021). Prediction of Fracture Distribution and Evaluation of Shale Gas Preservation Conditions in Longmaxi Formation in Dongxi Area. *Coal Geol. Explor.* 49 (6), 35–45. doi:10.3969/j.issn.1001-1986.2021.06.004

Yin, S., Tian, T., and Wu, Z. (2019). Developmental Characteristics and Distribution Law of Fractures in a Tight Sandstone Reservoir in a Low-Amplitude Tectonic Zone, Eastern Ordos Basin, China. *Geol. J.* 54, 1–16. doi:10.1002/gj.3521

Zhan, H., Yang, Y., Zhang, Y., Miao, X., Zhao, K., and Yue, W. (2021). Terahertz for the Detection of the Oil Bearing Characteristics of Shale. *Energy Rep.* 7, 5162–5167. doi:10.1016/j.egyr.2021.08.109

Zhang, L., Chen, L., Hu, R., and Cai, J. (2022). Subsurface Multiphase Reactive Flow in Geologic CO2 Storage: Key Impact Factors and Characterization Approaches. *Adv. Geo-Energy Res.* 6 (3), 179–180. doi:10.46690/ager.2022.03.01

Conflict of Interest: JL, JX, YW, and ZG were employed by the Institute of Geological Exploration and Development of CNPC Chuanqing Drilling Engineering.

The remaining author declares that the research was conducted in the absence of any commercial or financial relationships that could be construed as a potential conflict of interest.

Publisher's Note: All claims expressed in this article are solely those of the authors and do not necessarily represent those of their affiliated organizations, or those of the publisher, the editors and the reviewers. Any product that may be evaluated in this article, or claim that may be made by its manufacturer, is not guaranteed or endorsed by the publisher.